

*Letter to the Editor***Dense gas in nearby galaxies****XIV. Detection of hot ammonia in Maffei 2**C. Henkel<sup>1</sup>, R. Mauersberger<sup>2</sup>, A.B. Peck<sup>1</sup>, H. Falcke<sup>1</sup>, and Y. Hagiwara<sup>1</sup><sup>1</sup> Max-Planck-Institut für Radioastronomie, Auf dem Hügel 69, 53121 Bonn, Germany<sup>2</sup> Instituto de Radioastronomía Milimétrica, Avda. Divina Pastora, 7NC, 18012 Granada, Spain

Received 10 July 2000 / Accepted 7 September 2000

**Abstract.** The  $(J, K) = (1,1), (2,2), (3,3),$  and  $(4,4)$  inversion lines of ammonia ( $\text{NH}_3$ ) have been detected toward the nuclear  $40''$  sized bar of the nearby spiral galaxy Maffei 2. The relative intensities of the ammonia lines are characterized by a rotational temperature of 85 K. This is higher than rotational temperatures measured toward IC 342 and most Galactic Center clouds, implying kinetic temperatures  $\gtrsim 100$  K. Since the kinetic temperature of the gas is larger than that of the dust,  $\text{NH}_3$  is tracing a particularly dense warm gas component that is heated by young massive stars, cloud-cloud collisions, or ion-slip heating in the nuclear starburst. The gas north of the nucleus ( $V_{\text{LSR}} = -80 \text{ km s}^{-1}$ ) is more highly excited than the gas further south ( $+6 \text{ km s}^{-1}$ ). This asymmetry might be related to pronounced morphological distortions that are observed in the north-eastern part of the galaxy.

**Key words:** galaxies: individual: Maffei 2 – galaxies: ISM – radio lines: galaxies

**1. Introduction**

For the past decade, it has been possible to study the excitation of the molecular gas in external galaxies (e.g. Mauersberger & Henkel 1989; Mauersberger et al. 1990; Jackson et al. 1995; Hüttemeister et al. 1997; Paglione et al. 1997; Heikkilä et al. 1999; Mao et al. 2000). While the interpretation of CO emission often requires the application of complex models that incorporate temperature gradients at the surfaces of clouds, species like CS, HCN, or  $\text{HC}_3\text{N}$  trace higher density gas closer to the cloud cores and may thus be properly modeled with the standard ‘Large Velocity Gradient’ approach. Observed line intensity ratios of such high density tracers depend mostly on the number density  $n(\text{H}_2)$ , but also on the kinetic temperature  $T_{\text{kin}}$  of the gas. It is virtually impossible to disentangle these parameters, making observations of a molecule tracing exclusively temperature highly desirable.

*Send offprint requests to:* C. Henkel

Ammonia ( $\text{NH}_3$ ) is such a molecule. With a single telescope-receiver configuration at 18–26 GHz, a large number of  $\text{NH}_3$  inversion transitions can be measured, covering an enormous range of molecular excitation levels. These include the  $(J, K) = (1,1)$  to  $(4,4)$  inversion lines at 23, 65, 123, and 199 K above the ground state. Extragalactic ammonia was first detected in the  $(J, K) = (1,1)$  line toward the nearby face-on spiral IC 342 (Martin & Ho 1979). This was followed by detections of the  $(2,2), (3,3),$  and  $(4,4)$  lines (Ho et al. 1982, 1990; Martin & Ho 1986) that permitted a first estimate of the kinetic temperature of the dense nuclear gas in an external galaxy.

In view of the four ammonia lines observed toward IC 342 (the  $(6,6)$  line was also tentatively detected) it is surprising how little is known about ammonia in other external galaxies. Motivated by our unpublished detections of  $(J, K) = (1,1)$  and  $(2,2)$  emission in 1994 and by recent improvements in receiver sensitivity, baseline stability, and accessible bandwidth, we present a multilevel ammonia study of Maffei 2, an optically obscured barred spiral galaxy that is located behind the plane of the Milky Way at a distance of  $\sim 2.5$  Mpc (e.g. Karachentsev et al. 1997). High lower limits to the kinetic temperature of its dense nuclear gas are derived.

**2. Observations**

All data presented here were taken in March 2000, using the Effelsberg 100-m telescope of the MPIfR equipped with a dual channel K-band HEMT receiver. The system temperature was  $\sim 220$  K on a main beam brightness temperature scale; the beam size was  $\sim 40''$ . The data were recorded using an autocorrelator with  $8 \times 256$  channels and bandwidths of 80 MHz. The eight backends were configured in two groups of four, sampling data from both linear polarizations. Frequency shifts between the four backends representing a given linear polarization were adjusted in such a way that the  $(J, K) = (1,1)$  to  $(4,4)$  lines of ammonia could be measured simultaneously.

The measurements were carried out in a dual beam switching mode (switching frequency 1 Hz) with a beam throw of  $121''$  in azimuth. Calibration was obtained by measurements of the

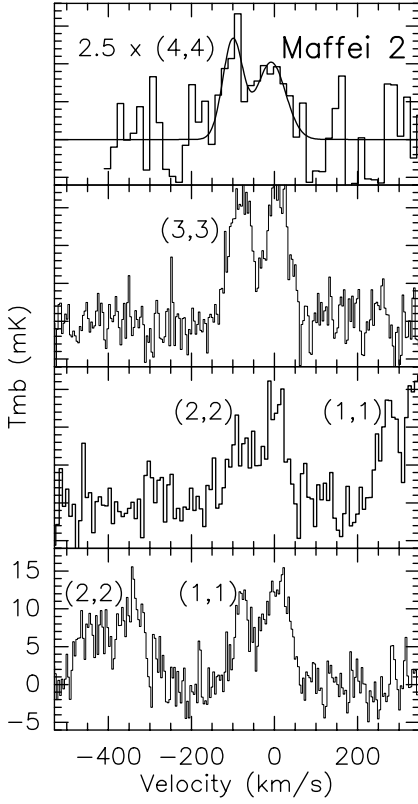


**Fig. 1.**  $\text{NH}_3$  spectra towards Maffei 2 ( $\alpha_{2000} = 2^{\text{h}} 41^{\text{m}} 55^{\text{s}}.1$ ,  $\delta_{2000} = +59^{\circ} 36' 12''$ ) after subtraction of linear baselines. Channel spacings are 3.9, 7.8, 3.9, and 15.7  $\text{km s}^{-1}$  for the  $(J, K) = (1,1)$  to  $(4,4)$  lines at 23694.496, 23722.631, 23870.130, and 24139.417 MHz, respectively. The  $\text{NH}_3$   $(4,4)$  spectrum, with the temperature scale multiplied by a factor of 2.5, is shown with a tentative gaussian decomposition.

radio continuum of W3(OH) and 3C 286 (for fluxes, see Baars et al. 1977; Mauersberger et al. 1988; Ott et al. 1994) and  $\text{NH}_3$  spectra of Orion-KL and IC 342 (Martin & Ho 1986; Hermsen et al. 1988). We estimate an absolute calibration accuracy of  $\pm 10\%$ . Relative calibration should be even more accurate, at the order of  $\pm 5\%$ . Pointing errors as well as weather or elevation dependent gain variations affect all lines in a similar way; the calibration signal injected by a noise diode shows little frequency dependence and remains stable (within at least 5%) over the observed frequency interval. Spectral intensities were converted to a main beam brightness temperature ( $T_{\text{mb}}$ ) scale. Pointing was checked every hour on nearby continuum sources and was found to be stable to within  $5\text{--}10''$ .

### 3. Results

Fig. 1 shows the measured spectra toward the central 0.5 kpc, displaying a velocity range between  $-530$  and  $+350$   $\text{km s}^{-1}$ . Line parameters are given in Table 1. The  $(1,1)$  to  $(3,3)$  lines are clearly detected; the  $(4,4)$  line is observed at a  $4.5\sigma$  level. The  $(1,1)$  to  $(3,3)$  profiles show two distinct velocity components, separated by  $\sim 85$   $\text{km s}^{-1}$ . In the  $(1,1)$  and  $(2,2)$  lines, the higher velocity component is stronger; in the  $(3,3)$  line, however, both

**Table 1.** Integrated line intensities ( $\int T_{\text{mb}} dv$ ), Local Standard of Rest velocities ( $V_{\text{LSR}}$ ), full width to half power linewidths ( $\Delta V_{1/2}$ ), and upper state column densities ( $2 \cdot N_{\text{u}}(J, K) \sim N(J, K)$ ) for the  $(1,1)$  to  $(4,4)$  lines of ammonia towards Maffei 2. Line parameters were obtained from gaussian fits to the data. Errors in Cols. 3 and 4 are standard deviations from the fit; Cols. 2 and 5 also include a 10% uncertainty in absolute calibration (see Sect. 2).

Transition ( $J, K$ )	$\int T_{\text{mb}} dv$ $\text{K km s}^{-1}$	$V_{\text{LSR}}$ $\text{km s}^{-1}$	$\Delta V_{1/2}$ $\text{km s}^{-1}$	$N_{\text{u}}(J, K)$ $10^{12} \text{ cm}^{-2}$
(1,1)	$0.527 \pm 0.080$	$-78 \pm 2$	$43 \pm 6$	$3.44 \pm 0.52$
(1,1)	$1.024 \pm 0.121$	$+6 \pm 2$	$70 \pm 5$	$6.69 \pm 0.78$
(2,2)	$0.694 \pm 0.122$	$-78 \pm 6$	$83 \pm 12$	$3.40 \pm 0.60$
(2,2)	$0.782 \pm 0.131$	$+5 \pm 4$	$66 \pm 10$	$3.83 \pm 0.63$
(3,3)	$1.127 \pm 0.131$	$-82 \pm 2$	$62 \pm 4$	$4.88 \pm 0.57$
(3,3)	$1.110 \pm 0.128$	$+8 \pm 2$	$56 \pm 4$	$4.80 \pm 0.55$
(4,4)	$0.882 \pm 0.215$	$-57 \pm 20$	$174 \pm 40$	$3.55 \pm 0.87$

components show similar line strength. In the  $(4,4)$  transition it is difficult to resolve the two features but the line center is closer to the velocity of the  $-80$   $\text{km s}^{-1}$  component (Table 1). This is also suggested by a tentative two component fit to the  $(4,4)$  line shown in Fig. 1, where 60–65% of the emission seems to arise from the  $-80$   $\text{km s}^{-1}$  component. We conclude that there is a trend with the  $-80$   $\text{km s}^{-1}$  component rising in relative strength with excitation above the ground state.

### 4. Determination of rotational temperatures

With  $h\nu/k \sim 1.14$  K and expected excitation temperatures  $\gtrsim 10$  K across an inversion doublet we obtain, in the optically thin case, beam averaged column densities of

$$N(J, K) = \frac{7.77 \cdot 10^{13}}{\nu} \frac{J(J+1)}{K^2} \int T_{\text{mb}} dv$$

for an individual inversion state. The column density  $N$ , the frequency  $\nu$ , and the integral are in units of  $\text{cm}^{-2}$ , GHz, and  $\text{K km s}^{-1}$ , respectively. Calculated column densities are displayed in the last column of Table 1. For our observed metastable ( $J = K$ ) inversion transitions, the rotational temperature  $T_{\text{rot}}$  between the states  $(J, J)$  and  $(J', J')$  can then be obtained from

$$\frac{N(J, J)}{N(J', J')} = \frac{g_{\text{op}}(J')}{g_{\text{op}}(J)} \frac{2J'+1}{2J+1} \exp\left(\frac{-\Delta E}{kT_{\text{rot}}}\right),$$

where  $g_{\text{op}} = 1$  for para-ammonia, i.e. for  $(J, K) = (1,1)$ ,  $(2,2)$ , and  $(4,4)$ , and  $g_{\text{op}} = 2$  for ortho-ammonia, i.e. for the  $(3,3)$  line.  $\Delta E$  is the energy difference between the states involved.

Rotation diagrams of the ammonia emission in the  $(1,1)$  to  $(4,4)$  lines are shown in Fig. 2. The  $(3,3)$  line, although belonging to a different ammonia species, fits well in the general trend of decreasing normalized column density with energy above the ground state. The slope of the lines fitting the normalized column densities is  $-\log e/T_{\text{rot}}$ . A weighted fit to the total ammonia emission (solid line; relative weights reflect signal-to-noise ratios) yields a rotational temperature of  $85 \pm 15$  K ( $1\sigma$

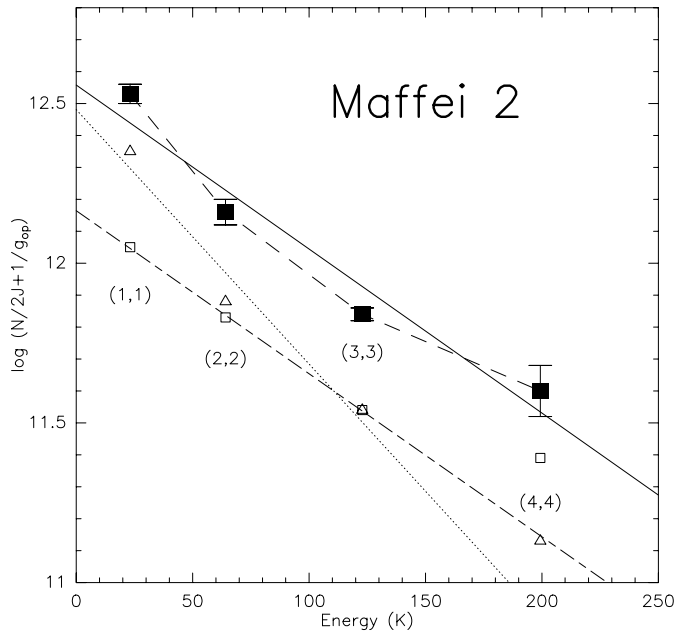


**Fig. 2.** A rotation diagram of metastable ammonia transitions towards Maffei 2, assuming optically thin emission and excitation temperatures  $\gg 2.7$  K for each inversion doublet. The column densities  $N$  from Table 1 refer to the upper state of the respective inversion doublet. Filled squares: Total emission (dashed line connects the points); empty squares:  $-80$  km s $^{-1}$  component; empty triangles:  $+6$  km s $^{-1}$  component. Straight lines provide best fits to the total emission in the  $(J, K) = (1,1) - (4,4)$  lines (solid) and to the  $(1,1) - (3,3)$  emission lines for the  $-80$  and  $+6$  km s $^{-1}$  components (dashed and dotted, respectively). The decomposition of the  $(4,4)$  line into two velocity components, based on the fit shown in Fig. 1, is at best only marginally significant. Errors for the individual  $(1,1)$  to  $(3,3)$  components are  $\sim 40\%$  larger than those for the total emission.

error). Excluding the  $(4,4)$  line from the fit gives  $65 \pm 10$  K. For the two velocity components, only including the  $(1,1)$  to  $(3,3)$  lines,  $T_{\text{rot}} = 85 \pm 5$  ( $V_{\text{LSR}} = -80$  km s $^{-1}$ ) and  $55 \pm 10$  K ( $V_{\text{LSR}} = +6$  km s $^{-1}$ ). Inclusion of the highly tentative decomposition of the  $(J, K) = (4,4)$  line (Fig. 1) yields  $T_{\text{rot}} \sim 115$  and  $65$  K. As sometimes observed in Galactic sources, the inclusion of higher excited inversion levels leads to higher rotational temperature estimates. This is indicated by the decreasing (negative) slope of the line connecting the measured points.

## 5. Discussion

### 5.1. Interpretation of rotational temperatures

The  $J = K$  ammonia inversion doublets are called metastable because they decay radiatively via slow  $\Delta K = \pm 3$  transitions. As a consequence, the relative population of these states is strongly affected by collisions and thus reflects (e.g. Walmsley & Ungerechts 1983) the kinetic temperature of the gas ( $T_{\text{rot}} \leq T_{\text{kin}}$ ).

One way to explain rising rotational temperatures with increasing energy above the ground state is the presence of kinetic temperature gradients. Alternatively, optically thick lines

or subthermal excitation can produce the same effect (Goldsmith & Langer 1999). Accounting for these latter two effects, radiative transfer calculations (e.g. Walmsley & Ungerechts 1983; Schilke 1989) predict that rotational temperatures approach the kinetic temperature with rising energy of the analysed metastable inversion doublets. This yields rising  $T_{\text{rot}}$  with rising  $E/k$ . It is therefore likely, based on the corrections of the models, that the true kinetic temperature is  $> 100$  K.  $T_{\text{kin}}$  should be larger for the  $-80$  than for the  $+6$  km s $^{-1}$  velocity component.

### 5.2. A comparison with IC 342 and Galactic Center clouds

$\text{NH}_3$  integrated line temperatures are larger towards Maffei 2 than towards IC 342, also located at  $D \sim 2.5$  Mpc (Karachentsev et al. 1997). Emission from the inner 500 pc of the Milky Way would show similar intensities if observed from this distance (e.g. Hüttemeister et al. 1993a,b).

From the  $(J, K) = (1,1)$  to  $(4,4)$  lines,  $T_{\text{rot}} \sim 85$  K in Maffei 2, but only  $50 \pm 10$  K in IC 342 (Martin & Ho 1986). Toward peak positions of clouds near the center of the Galaxy,  $(1,1)$  lines tend to be optically thick, while more highly excited inversion lines show no significant optical depth effects (Hüttemeister et al. 1993b). There are two main temperature components, one at  $T_{\text{kin}} \sim 25$  and one at  $\sim 200$  K. These, if present in Maffei 2 as well, could be responsible for the increasing rotational temperatures with  $E/k$  (Fig. 2). Such gradients are also seen in IC 342, if the  $(6,6)$  line is as strong as suggested by the spectrum presented by Martin & Ho (1986).

### 5.3. The nuclear region of Maffei 2

What kind of molecular gas is seen in ammonia? Critical densities, where collisional de-excitation matches spontaneous emission rates, are  $n(\text{H}_2) \sim 3 \cdot 10^3$  cm $^{-3}$  (e.g. Green 1980; Ho & Townes 1983). Our beam size ( $40''$ ) matches the central bar with its size of  $43'' \times 9''$  in  $^{12}\text{CO } J = 1-0$  (Ishiguro et al. 1989) and  $40'' \times 12''$  in  $^{13}\text{CO } J = 1-0$  (Hurt & Turner 1991). The presence of bars provides a viable mechanism to transfer interstellar gas into the nuclear region of a galaxy, leading to the formation of dense molecular clouds and triggering bursts of star formation. As long as the gas is not yet fully ionized or swept away by stellar winds, it will coexist with the newly formed stars and will be heated by their radiation, by an enhanced flux of cosmic rays, by cloud-cloud collisions, and by the dissipation of turbulent energy. Both Maffei 2 and IC 342 show prominent nuclear bars and strong CO, infrared, and radio continuum emission (e.g. Lo et al. 1984; Ishiguro et al. 1989; Ishizuki et al. 1990; Hurt & Turner 1991; Turner & Ho 1994; Meier et al. 2000).

Assuming a grain emissivity law of  $\lambda^{-1}$ , dust temperatures deduced from the Kuiper Airborne Observatory and, for a larger region, from IRAS data (Rickard & Harvey 1983; IRAS 1989) are  $T_{\text{d}} = 33-47$  K. Ignoring non-metastable inversion doublets, Table 1 implies that  $N(\text{NH}_3)$  is on the order of  $10^{14}$  cm $^{-2}$ . For  $\text{H}_2$ , with  $D = 2.5$  Mpc,  $N(\text{H}_2) \sim 10^{22}$  cm $^{-2}$  (Hurt & Turner 1991). This yields a relative abundance of  $X(\text{NH}_3) \sim 10^{-8}$ . With  $T_{\text{rot}}(\text{NH}_3) \gg T_{\text{d}}$  and an unusually small  $\text{NH}_3$  abundance (e.g.

Benson & Myers 1983; Brown et al. 1988), ammonia should trace a gas component that is different from that seen in CO (for an analysis of CO emission in a nuclear starburst environment, see Mao et al. 2000). Cloud-cloud collisions, young massive stars, or ion-slip heating (Hüttemeister et al. 1993a,b) may cause the high rotational temperatures. SiO, an exclusive tracer of high temperature gas, was detected in Maffei 2 (Sage & Ziurys 1995) and is likely arising from the same gas component. Detailed studies of NH<sub>3</sub> and SiO in the Galactic Center region (e.g. Hüttemeister et al. 1993a,b, 1998) indicate that the warm gas not directly associated with massive stars is only moderately dense ( $n(\text{H}_2) \sim 5 \cdot 10^3 \text{ cm}^{-3}$ ).

From a comparison with the interferometric maps of Ishiguro et al. (1989) and Hurt & Turner (1991), the ammonia component at +6 kms must arise SW, the  $-80 \text{ km s}^{-1}$  component NE of the center of the galaxy. Why is the rotation diagram (Fig. 2) indicating higher excitation NE of the nucleus? The bar in Maffei 2 may be caused by a merger with a satellite galaxy in the NE that severely disrupts this side of the galaxy (Hurt et al. 1996). This might have led to differences in inflow rates, star forming rates, and gas heating at the north-eastern and south-western sides of the nucleus. While our observed small scale ( $\sim 500 \text{ pc}$ ) nuclear asymmetry in rotational temperature may be consistent with the large scale asymmetry observed in HI, the proposed connection between these phenomena remains speculative. More data on the putative interacting dwarf galaxy, detailed simulations of the interaction, and models of the evolution of the nuclear bar are needed to verify or to reject the proposed scenario and to explain the recent past of Maffei 2.

*Acknowledgements.* We wish to thank J.L. Turner for critically reading the manuscript.

## References

- Baars J.W.M., Genzel R., Pauliny-Toth I.I.K., Witzel A., 1977, A&A 61, 99
- Benson P.J., Myers P.C., 1983, ApJ 270, 589
- Brown P.D., Charnley S.B., Millar T.J., 1988, MNRAS 231, 409
- Goldsmith P.F., Langer W.D., 1999, ApJ 517, 209
- Green S., 1980, J. Chem. Phys. 73, 2740
- Heikkilä A., Johansson L.E.B., Olofsson H., 1999, A&A 344, 817
- Hermesen W., Wilson T.L., Walmsley C.M., Henkel C., 1988, A&A 201, 285
- Ho P.T.P., Townes C.H., 1983, ARA&A 21, 239
- Ho P.T.P., Martin R.N., Ruf K., 1982, A&A 113, 155
- Ho P.T.P., Martin R.N., Turner J.L., Jackson J.M., 1990, ApJ 355, L19
- Hurt R.L., Turner J.L., 1991, ApJ 377, 434
- Hurt R.L., Turner J.L., Ho P.T.P., 1996, ApJ 466, 135
- Hüttemeister S., Wilson T.L., Henkel C., Mauersberger R., 1993a, A&A 276, 445
- Hüttemeister S., Wilson T.L., Bania T.M., Martín-Pintado J., 1993b, A&A 280, 255
- Hüttemeister S., Mauersberger R., Henkel C., 1997, A&A 326, 59
- Hüttemeister S., Dahmen G., Mauersberger R. et al., 1998, A&A 334, 646
- IRAS Point Source Catalog, Cataloged Galaxies and Quasars observed in the IRAS Survey, Version 2.0, L. Fullmer & C. Lonsdale, 1989
- Ishiguro M., Kawabe R., Morita K.-I. et al., 1989, ApJ 344, 763
- Ishizuki S., Kawabe R., Ishiguro M. et al., 1990, Nat 344, 224
- Jackson J.M., Paglione T.A.D., Carlstrom J.E., Nguyen-Q-Rieu, 1995, ApJ 438, 695
- Karachentsev I., Drozdovsky I., Kajsins S. et al., 1997, A&AS 124, 559
- Lo K.-Y., Berge G.L., Claussen M.J. et al., 1984, ApJ 282, L59
- Mao R.Q., Henkel C., Schulz A. et al., 2000, A&A 358, 433
- Martin R.N., Ho P.T.P., 1979, A&A 74, L7
- Martin R.N., Ho P.T.P., 1986, ApJ 308, L7
- Mauersberger R., Henkel C., 1989, A&A 223, 79
- Mauersberger R., Wilson T.L., Henkel C., 1988, A&A 201, 123
- Mauersberger R., Henkel C., Sage L.J., 1990, A&A 236, 63
- Meier D.S., Turner J.L., Hurt R.L., 2000, ApJ 531, 200
- Ott M., Witzel A., Quirrenbach A. et al., 1994, A&A 284, 331
- Paglione T.A.D., Jackson J.M., Ishizuki S., 1997, ApJ 484, 656
- Rickard L.J., Harvey P.M., 1983, ApJ 268, L7
- Sage L.J., Ziurys L.M., 1995, ApJ 447, 625
- Schilke P., 1989, Diploma Thesis, Univ. of Bonn
- Turner J.L., Ho P.T.P., 1994, ApJ 421, 122
- Walmsley C.M., Ungerechts H., 1983, A&A 122, 164